

559191  
31P

GRANT/TR/IN/47

2002 018 943

**Observations of three-dimensional radiative effects that influence  
satellite retrievals of cloud properties**

**Tamás Várnai and Alexander Marshak**  
*Joint Center for Earth Systems Technology of  
University of Maryland, Baltimore County, and  
NASA Goddard Space Flight Center*

Prepared for *Időjárás*  
October 2, 2001

*Corresponding author address:* Tamás Várnai, Code 913, NASA GSFC, Greenbelt, MD  
20771, USA. E-mail: varnai@climate.gsfc.nasa.gov

## **Abstract**

This paper examines three-dimensional (3D) radiative effects, which arise from horizontal radiative interactions between areas that have different cloud properties. Earlier studies have argued that these effects can cause significant uncertainties in current satellite retrievals of cloud properties, because the retrievals rely on one-dimensional (1D) theory and do not consider the effects of horizontal changes in cloud properties. This study addresses two questions: which retrieved cloud properties are influenced by 3D radiative effects, and where 3D effects tend to occur. The influence of 3D effects is detected from the way side illumination and shadowing make clouds appear asymmetric: Areas appear brighter if the cloud top surface is tilted toward, rather than away from, the sun. The analysis of 30 images by the Moderate Resolution Imaging Spectroradiometer (MODIS) reveals that retrievals of cloud optical thickness and cloud water content are most influenced by 3D effects, whereas retrievals of cloud particle size are much less affected. The results also indicate that while 3D effects are strongest at cloud edges, cloud top variability in cloud interiors, even in overcast regions, also produces considerable 3D effects. Finally, significant 3D effects are found in a wide variety of situations, ranging from thin clouds to thick ones and from low clouds to high ones.

I am very happy to be able to contribute to this special issue honoring Dr. Major. I am deeply grateful to him for his support throughout my years at the Hungarian Meteorological Service, and for his help when I applied to graduate school.

Tamás Várnai

## **1. Introduction**

Satellite measurements are often used to infer various cloud properties, such as the clouds' water content or particle size. Currently, the calculations assume that when a satellite measures the solar radiation reflected from a particular area of a cloud, the characteristics of this radiation are shaped by the cloud properties in that area only. In other words, the calculations rely on one-dimensional (1D) radiative transfer theory: They interpret the radiances measured at a particular pixel by assuming that the pixel's surroundings have identical cloud properties, with no changes in horizontal directions. This approach has the advantage of allowing an unambiguous interpretation of the measured radiance values, leading to a single set of estimated cloud properties. In contrast, if the full three-dimensional (3D) radiative transfer were considered (including horizontal interactions between areas that have different cloud properties), the radiances measured at a pixel could correspond to a variety of cloud properties: For example, a thin cloud could be as bright as a thicker cloud that was shaded by an even thicker cloud.

Since the mid-1980s, numerous theoretical studies have indicated that the 1D approximation can cause significant errors in satellite retrievals and that 3D radiative effects must also be considered (e.g., Davies 1984; Kobayashi 1993; Barker and Liu

1995). Simulation results have indicated that, depending on the circumstances, 1D retrievals can yield clouds that are too thin or too thick, too rough or too smooth, artificially anisotropic, and asymmetric (e.g., Marshak et al. 1995; Zuidema and Evans 1998; Várnai 2000). Unfortunately, detecting the influence of 3D effects in actual observations has proven to be a much more elusive task, mainly because of the difficulties in separating the influence of 3D effects from uncertainties in other factors, such as variations in cloud droplet size. The lack of observational evidence made it difficult to tell whether the 3D effects suggested by theoretical results really occur in the atmosphere. The main question has been not whether 3D radiative processes are calculated correctly for the clouds considered in theoretical studies, but whether the simulated clouds have realistic horizontal variability.

The first unambiguous observations of 3D effects emerged in the mid-1990s. First, several studies examining 30 m-resolution Landsat images found that for high sun, the diffusion of radiation inside clouds smoothes out small-scale variability—and so clouds appear more homogeneous than they really are (Marshak et al. 1995; Davis et al. 1997; Oreopoulos et al. 2000). Around the same time, the statistical analysis of satellite data at resolutions ranging from 1 km to 30 km revealed that 3D effects make clouds appear too thick when the sun is very oblique (Loeb and Davies 1996; Loeb and Coakley 1998). In addition, new multiangle satellite measurements revealed that cloud reflection into forward oblique view directions is smaller than expected from 1D theory—and that the reduction can be caused by 3D effects (Buriez et al. 2001; Ákos Horváth, Iliana Genkova and Roger Davies 2001, personal communication). Most recently, Várnai and Marshak (2001) found a clear signal of 3D effects for moderately oblique solar

illumination: Side illumination and shadowing effects make clouds appear asymmetric, as if clouds were brighter and thicker on their side facing the sun than on the opposite side. This effect makes it more difficult to combine the satellite data with ground-based or airborne measurements on a pixel-by-pixel basis, distorts the histogram of retrieved cloud properties, and makes clouds appear rougher than they really are. On the positive side, theoretical simulations by Várnai and Marshak (2001) indicated that the observed asymmetry is closely related to the way 3D effects change the average cloud reflection of large areas—which suggests that one can use the observed asymmetry values to estimate the large-scale retrieval biases due to 3D effects.

The goal of this paper is to analyze observations of apparent cloud asymmetry in order to gain new insights into 3D radiative effects. First, Section 2 describes the satellite data used in this study and briefly discusses how the apparent cloud asymmetry is determined from the observations. Section 3 then analyzes the observations to see which retrieved cloud properties are influenced by 3D effects and to better understand in which clouds 3D effects tend to occur. Finally Section 4 offers a brief summary and a few concluding remarks.

## **2. Data and methodology**

### **2.1 Satellite data used**

This study uses measurements by the Moderate Resolution Imaging Spectroradiometer (MODIS) instrument on board the Terra satellite. Terra was launched

on a polar sun-synchronous orbit in December 1999, and it orbits the Earth in 98 minutes with a 10:30 a.m. equatorial crossing time at a 705 km altitude. MODIS is a precursor instrument to the next generation of imagers that will replace the Advanced Very High Resolution Radiometers (AVHRR) on the operational polar-orbiting satellites of the National Oceanic and Atmospheric Administration (NOAA). MODIS takes measurements at 36 wavelengths ranging from 0.4 to 14.4  $\mu\text{m}$ . The spatial resolution at the subsatellite point is 250 m, 500 m, or 1 km, depending on the wavelength. This study uses 1 km resolution data from two wavelengths, 0.86  $\mu\text{m}$  and 11  $\mu\text{m}$ . The 0.86  $\mu\text{m}$  radiances are converted to reflectances ( $R$ ) using the equation

$$R = \frac{\pi \cdot I}{\cos \Theta_0 \cdot F_0}, \quad (1)$$

where  $I$  is the radiance,  $\Theta_0$  is the solar zenith angle, and  $F_0$  is the solar constant. The 11  $\mu\text{m}$  radiances are transformed into equivalent brightness temperature values using the Planck formula (e.g., Thomas and Stamnes 1999, p. 94).

Although AVHRR and other instruments also offer measurements at similar wavelengths, MODIS is particularly well suited for this study because of its high radiometric accuracy. Especially important is the sensitivity at 11  $\mu\text{m}$ , because observations of small temperature changes are crucial for the adopted methodology. (MODIS images report temperature changes as small as 0.01 K, and the noise equivalent temperature difference is around 0.05 K (NASA 2000).)

In addition to using radiance measurements, this study also uses some standard MODIS products freely available at [http://daac.gsfc.nasa.gov/CAMPAIGN\\_DOCS/MODIS/index.shtml](http://daac.gsfc.nasa.gov/CAMPAIGN_DOCS/MODIS/index.shtml). In particular, we used the 1 km-resolution cloud optical thickness, cloud water path, and cloud particle size

data; the 5 km–resolution land-water mask; and the solar and viewing zenith and azimuth angles.

MODIS data are distributed in approximately 2000 km by 2000 km segments called granules. This study used the central 450 km–wide portion of 30 granules, where the viewing zenith angle is less than  $20^\circ$ . This restriction eliminates potential difficulties that could arise for oblique views, such as areas being viewed twice or pixel sizes increasing. The 30 granules were taken from three days separated by 10-day intervals: May 14, May 25, and June 4, 2001. The 10-day separation ensures that the images are relatively independent from each other, because the weather systems observed on one day are not likely to still exist 10 days later. Ten granules were taken from each day—essentially all granules that satisfy the following two criteria. First, the central portion of the granule should cover mostly oceanic areas. This is helpful because cloud detection and cloud property retrievals are easier and more accurate over ocean than over land. Second, the sun should be moderately oblique, with solar zenith angles around  $60^\circ$ . (Due to the large size of MODIS images, the actual zenith angles vary between  $45^\circ$  and  $75^\circ$ , but they remain close to  $60^\circ$  most of the time.) Because of the Terra satellite’s sun-synchronous orbit, this requirement implies that all granules are around  $35^\circ$  S latitude. Let us note that the images are from a similar season and latitude band as in Várnai and Marshak (2001)—which used images from November 2000 around  $40^\circ$  N latitude—but from the southern hemisphere. The specific granules used in this study are listed in Table 1.

## **2.2 Calculation of the apparent cloud asymmetry**

This study follows the methodology described in Várnai and Marshak (2001). The method's basic assumption is that if the cloud top surface is not horizontal (as assumed in 1D theory), 3D radiative effects make pixels brighter or darker than they would be in 1D theory. The brightening or darkening is expected to come from changes in the solar illumination, depending on whether the cloud top is tilted toward or away from the sun. For any given  $(1 \text{ km})^2$  cloudy pixel—for which the operational MODIS data processing retrieved a nonzero cloud optical thickness—the direction of the cloud slope is determined in two steps. First, Step 1 determines which two neighboring pixels in front and behind are closest to the solar azimuth. Step 2 then compares the  $11 \text{ }\mu\text{m}$  brightness temperatures ( $T$ ) of these two neighbors. Because temperature tends to decrease with altitude, Step 2 declares that our pixel is on a slope tilted toward the sun if  $T_{\text{front}} > T_{\text{behind}}$  and that it is on a slope tilted away from the sun if  $T_{\text{front}} < T_{\text{behind}}$ . Following Várnai and Marshak (2001), the two kinds of pixels will be identified as *illuminated* (subscript  $i$ ) or *shadowy* (subscript  $s$ ), even though no actual shadows are required for a pixel to be designated as shadowy.

Let us note that this designation can be made for pixels at local temperature minima and maxima as well, and even for pixels at cloud edges. The only exception is if both the neighbors in front and behind are cloud free—that is, if a single pixel contains both the illuminated and shadowy sides of a cloud. For such “isolated” pixels, the relationship between  $T_{\text{front}}$  and  $T_{\text{behind}}$  has much more to do with conditions at ground level than at the cloud top—and so these pixels are not considered in our calculations.

Fortunately, such isolated pixels occur quite rarely: In the examined scenes, fewer than 2% of all cloudy pixels fall into this category.

Once all cloudy  $(1 \text{ km})^2$  pixels in a  $(50 \text{ km})^2$  area are designated as either illuminated or shadowy, the method compares the mean cloud properties of all illuminated pixels to the mean properties of all shadowy pixels. If the two mean values are close to each other, this indicates that 3D effects do not make much of a difference. If, however, there are large differences (e.g., if illuminated pixels are much brighter than shadowy pixels), then 3D effects are expected to be strong.

The approach described above assumes that the solar azimuth does not influence cloud development, and so the illuminated and shadowy slopes have statistically similar true cloud properties. One can argue that if 3D radiative effects did influence cloud development, the most likely consequence would be the enhancement and reduction in absorption at illuminated and shadowy slopes, respectively. This would make clouds geometrically asymmetric by making the buoyancy conditions different on the opposite clouds sides. The resulting asymmetries in cloud top altitude should then make the brightness temperature fields asymmetric as well. Figure 1, however, indicates that the brightness temperatures of illuminated and shadowy slopes are statistically identical, which suggests that 3D effects did not have a strong influence on the vertical growth of clouds. (Another possible consequence of 3D effects would be that the enhanced absorption in illuminated slopes could reduce droplet size through increased evaporation. Section 3, however, will show that this effect is not very large either.) Naturally, random processes (such as wind shear or the overlap of two cloud layers) can make clouds asymmetric in any particular area, but these effects should even out when a large number

of areas are considered. As a result, if we see that the illuminated portions of  $(50 \text{ km})^2$  areas are systematically brighter than their shadowy portions, 3D effects must be responsible for the systematic difference.

### 3. Observations of 3D radiative effects

#### 3.1 Analysis of 3D effects in retrievals of various cloud properties

Figure 2 compares the  $0.86 \mu\text{m}$  reflectances observed at illuminated and shadowy slopes. The figure clearly indicates that 3D effects are important in the examined scenes; the illuminated slopes are much brighter than the shadowy slopes. This intuitive tendency is in clear contrast to the behavior of  $11 \mu\text{m}$  brightness temperatures in Fig. 1.

Figure 3 shows that the 3D effects in Fig. 2 have a strong influence on optical thickness ( $\tau$ ) retrievals, which estimate much larger  $\tau$  values at slopes tilted toward the sun. It is interesting to note that the asymmetries in Fig. 3 are about twice as strong as in Várnai and Marshak (2001): The median relative difference between  $\bar{\tau}_i$  and  $\bar{\tau}_s$  is 26%, as opposed to the 13% in the earlier study. (The mean relative difference is 28%.) The discrepancy is probably related to differences in the distribution of cloud types in the two studies: Flat stratiform clouds that are close to the 1D ideal appear to be more frequent around  $40^\circ \text{ N}$  in November (in the earlier study), whereas the bumpier convective clouds that cause stronger 3D effects are more frequent around  $35^\circ \text{ S}$  in May (in this study). The differences indicate large regional or interannual variations in 3D radiative effects, and

they highlight the need for comprehensive studies on the climatological distribution of 3D effects.

Figure 4 indicates that retrievals of the effective particle size ( $r_{\text{eff}}$ ) are influenced much less than, and in the opposite direction from,  $\tau$  retrievals. The main reason for the opposite behavior is illustrated in Fig. 5, which depicts the way particle size is retrieved from pairs of reflectance measurements at 0.86 and 2.12  $\mu\text{m}$ . The retrievals use the algorithm of Nakajima and King (1990) to take advantage of the fact that absorption, and hence reflectance, depend strongly on droplet size. To explain the asymmetry in Fig. 4, let us assume that if 3D effects enhance the illumination of a pixel on an illuminated slope by a certain percentage, the 0.86 and 2.12  $\mu\text{m}$  reflectances increase by a similar percentage. For example, if the true properties of the pixel put it at point A in Fig. 5 according to 1D theory, side illumination moves it to point B along the dashed line. The enhanced 2.12  $\mu\text{m}$  reflectance is then interpreted by the 1D retrievals as if cloud absorption were smaller, that is, as if cloud droplets were smaller. On shadowy slopes the retrievals make the opposite error, thinking that the droplets are larger there. This overestimation of droplet size is further strengthened by the fact that absorption allows less 2.12  $\mu\text{m}$  than 0.86  $\mu\text{m}$  radiation to flow from the illuminated to the shadowy side inside the clouds, and so the 2.12  $\mu\text{m}$  reflectance is actually reduced by a larger percentage than the 0.86  $\mu\text{m}$  reflectance in shadowy slopes.

An additional factor contributing to the trend in Fig. 4 may be that—as mentioned in Section 2.2—the enhanced absorption at illuminated slopes strengthens the local radiative heating, and this increase weakens the condensational growth of cloud droplets on these slopes. Because, however, the combined effect of all these factors is quite small

(about 1 to 2  $\mu\text{m}$ ), neither one of the contributing factors appears to be particularly strong.

After retrieving  $\tau$  and  $r_{\text{eff}}$ , the operational MODIS data processing uses the results to calculate the clouds' water content (water path, or WP) from the equation

$$WP = \frac{2}{3} \rho \cdot \tau \cdot r_{\text{eff}}, \quad (2)$$

where  $\rho$  is the density of water (King et al., 1997). Since Figs. 3 and 4 show that 3D effects have a much stronger influence on retrievals of  $\tau$  than of  $r_{\text{eff}}$ , it is not surprising that the water path—which is a product of  $\tau$  and  $r_{\text{eff}}$ —shows a behavior similar to that of  $\tau$  (Fig. 6). The median relative difference between the water path of illuminated and shadowy slopes is 23%.

Because theoretical simulations in Várnai and Marshak (2001) indicated that the observed asymmetries are closely related to the area-averaged biases caused by 3D effects, we can conclude that the results discussed above indicate that 3D effects introduce the largest errors in retrievals of  $\tau$  and WP, whereas the retrievals of  $r_{\text{eff}}$  are much less affected.

### 3.2 Examination of where 3D radiative effects occur

Although the possibility of random asymmetries in true cloud properties prevents our technique from locating 3D radiative effects on a pixel-by-pixel basis, the technique can nevertheless yield valuable statistical information on where 3D effects tend to occur. One important question is whether 3D radiative effects are limited to some specific situations, or whether they occur under a wide range of circumstances. To address this

question, Fig. 7 plots the relative difference between the  $(50 \text{ km})^2$  average water path values retrieved for illuminated and shadowy pixels, as a function of the mean optical thickness of the  $(50 \text{ km})^2$  areas. The figure indicates that the relative difference increases rapidly until about  $\tau \approx 5$ , as multiple scattering (essential for any 3D effects) becomes more and more important. Once cloud reflection gets dominated by multiple scattering, however, the relative differences remain fairly constant. On one hand, this means that the absolute magnitude of 3D effects increases with cloud reflectance. On the other hand, the results reveal that clouds in a wide range of optical thicknesses are similarly effective in causing 3D radiative effects.

One can also use the available data to examine how 3D effects depend on cloud altitude. For this, Fig. 8 displays the overall average water path of all  $(1 \text{ km})^2$  illuminated and shadowy pixels (combined over all 30 scenes) as a function of cloud top pressure. (This pressure value is reported in the operational MODIS cloud product.) The figure reveals that average cloud thickness tends to increase with altitude—which is consistent with the idea that convective clouds contain more water as they grow taller. Although the absolute magnitude of 3D effects ( $WP_i - WP_s$ ) increases with altitude accordingly, the inset reveals that clouds in a wide range of altitudes are similarly effective in creating strong 3D effects and that low-level clouds in the boundary layer are the most effective ones.

Finally, let us examine how 3D effects depend on cloud brokenness. For this, Fig. 9 plots the relative difference between the area average values for  $WP_i$  and  $WP_s$  as a function of the cloud coverage in  $(50 \text{ km})^2$  areas. Although the cloud coverage is not a very good indicator of cloud brokenness (for example, 50% cloud coverage can occur not

only in truly broken scenes, but also at the edges of large overcast cloud fields), the figure has two interesting features: It shows that 3D effects are quite important even in overcast scenes and that 3D effects become even stronger in broken clouds. These results suggest that cloud edges may be more effective than areas inside the cloud at creating 3D effects, but cloud top variations are also very important. These conclusions are confirmed clearly in Fig. 10, which displays the difference between the overall average  $WP_i$  and  $WP_s$  values (combined over all 30 scenes) as a function of the cloudy pixels' distance to the closest cloud-free pixel. As expected, the differences are largest right at the cloud edges, but they remain significant even in the interior of clouds.

#### 4. Summary

This study examined three-dimensional (3D) radiative effects, which arise from horizontal radiative interactions between areas that have different cloud properties. Current methods of retrieving cloud properties from satellite measurements do not consider these effects, because the retrievals rely on one-dimensional (1D) radiative transfer theory—that is, they treat each pixel as if it were surrounded by identical pixels, without any changes in horizontal directions. Although the 1D approximation has the advantage of allowing an unambiguous interpretation of the radiances measured at a given pixel, numerous studies have argued that not considering 3D effects can cause problems in the retrievals. This paper focused on two particular questions: which retrieved cloud properties are most influenced by 3D radiative effects, and where 3D effects tend to occur.

To address these questions, the study examined 30 images, 2000 km by 450 km each, by the Moderate Resolution Imaging Spectroradiometer (MODIS), which were taken in May and June 2001 over oceans around 35° S latitude. The images were analyzed using the method proposed in Várnai and Marshak (2001). The method's basic idea is that if 3D effects are present in a scene, they make areas tilted toward the sun better illuminated—and consequently brighter—than the areas tilted away from the sun. This can result in systematic differences between the two kinds of areas, causing systematic asymmetries in the retrieved cloud properties. Thus, the method examines 3D effects by first estimating the tilt of cloud top surfaces from thermal infrared images, and then comparing the cloud properties retrieved for the two kinds of slopes.

The results revealed that 3D effects cause quite large uncertainties in the retrievals of cloud optical thickness and cloud water path: The median (and mean) difference between the values retrieved for areas tilted toward and away from the sun was about 25%. This result highlights that there are large regional differences in the importance of 3D effects, because, when Várnai and Marshak (2001) examined optical thickness fields, they found 3D effects only about half this strong in a similar season and latitude band in the northern hemisphere. In contrast, the present study found cloud particle size retrievals to be much less influenced by 3D effects: On average, droplet sizes were only about 1 to 2  $\mu\text{m}$  larger on slopes that are tilted away, rather than toward, the sun.

The results also revealed that 3D radiative effects are not limited to some narrow range of situations or cloud types, because 3D effects remained significant over a wide range of cloud thicknesses and cloud top altitudes.

Finally, the results showed that although cloud edges are most effective in causing 3D radiative effects, cloud top variability is nearly as important. Consequently, 3D effects were found to be strongest in broken clouds, but they were quite significant even in large overcast regions.

Overall, the results highlight that the 1D approximation is a significant limitation in current techniques that retrieve cloud properties from shortwave satellite measurements. Because the simulation results of Várnai and Marshak (2001) indicate that the observed consequence of 3D radiative interactions (the apparent cloud asymmetry) is closely related to other consequences of 3D effects, the presented results have implications for a wide range of issues, from the interpretation of satellite measurements to the modeling of photochemical processes. The abundance of 3D effects indicates that radiative transfer in cloudy atmospheres is an inherently 3D process, and it highlights the need for new radiative transfer models that can move beyond the 1D framework both in remote sensing and in other applications involving radiative transfer calculations.

*Acknowledgments* We appreciate funding for this research from the NASA EOS Project Science Office (under Grant NAG5-6675) and support from project scientist David O'C. Starr. We also thank Laura L. Atwood for proofreading the manuscript and providing helpful suggestions.

## References

- Barker, H. W., and D. Liu, 1995: Inferring optical depth of broken clouds from Landsat data. *J. Climate*, **8**, 2620–2630.
- Buriez, J.-C., M. Dutriaux-Biucher, F. Parol, and N. G. Loeb, 2001: Angular variability of the liquid water cloud optical thickness retrieved from ADEOS-POLDER. *J. Atmos. Sci.*, **58**, 3007–3018.
- Davies, R., 1984: Reflected solar radiances from broken cloud scenes and the interpretation of satellite measurements. *J. Geophys. Res.*, **89**, 1259–1266.
- Davis, A., A. Marshak, R. Cahalan, and W. Wiscombe, 1997: The Landsat scale-break in stratocumulus as a three-dimensional radiative transfer effect, implications for cloud remote sensing. *J. Atmos. Sci.*, **54**, 241–260.
- King, M. D., S.-C. Tsay, S. Platnick, M. Wang, and K.-N. Liou, 1997: *Cloud retrieval algorithms for MODIS: Optical thickness, effective particle radius, and thermodynamic phase*. MODIS Algorithm Theoretical Basis Document No. ATBD-MOD-05, Version 5, NASA.
- Kobayashi, T., 1993: Effects due to cloud geometry on biases in the albedo derived from radiance measurements. *J. Climate*, **6**, 120–128.
- Loeb, N. G., and R. Davies, 1996: Observational evidence of plane parallel model biases: Apparent dependence of cloud optical depth on solar zenith angle. *J. Geophys. Res.*, **101**, 1621–1634.
- Loeb, N. G., and J. A. Coakley, 1998: Inference of marine stratus cloud optical depths from satellite measurements: Does 1D theory apply? *J. Climate*, **11**, 215–233.

- Marshak, A., A. Davis, W. Wiscombe, and R. Cahalan, 1995: Radiative smoothing in fractal clouds. *J. Geophys. Res.*, **100**, 26,247–26,261.
- Nakajima, T. Y., and M. D. King, 1990: Determination of the optical thickness and effective radius of clouds from reflected solar radiation measurements. Part I: Theory. *J. Atmos. Sci.*, **47**, 1878–1893.
- NASA, 2000: *MODIS—Moderate Resolution Imaging Spectroradiometer*. Available from [http://modarch.gsfc.nasa.gov/MODIS/INSTRUMENT/modis\\_brochure.pdf](http://modarch.gsfc.nasa.gov/MODIS/INSTRUMENT/modis_brochure.pdf)
- Oreopoulos, L., A. Marshak, R. F. Cahalan, and G. Wen, 2000: Cloud 3D effects evidenced in Landsat spatial power spectra and autocorrelation functions. *J. Geophys. Res.*, **105**, 14,777–14,788.
- Thomas, G. E., and K. Stamnes, 1999: *Radiative Transfer in the Atmosphere and in the Ocean*. Cambridge University Press, 517 pp.
- Várnai, T., 2000: Influence of three-dimensional radiative effects on the spatial distribution of shortwave cloud reflection. *J. Atmos. Sci.*, **57**, 216–229.
- Várnai, T., and A. Marshak, 2001: Observations of three-dimensional radiative effects that influence MODIS cloud optical thickness retrievals. Submitted to *J. Atmos. Sci.*
- Zuidema, P., and K. F. Evans, 1998: On the validity of the Independent Pixel Approximation for the boundary layer clouds observed during ASTEX. *J. Geophys. Res.*, **103**, 6059–6074.

## Tables

Table 1. Dates and UTC times (hour:minute) that identify the granules used in this study.

Date	Time
May 14, 2001	03:20, 05:00, 06:40, 09:55, 11:35, 16:30, 18:10, 19:50, 21:30, 23:05
May 25, 2001	01:25, 03:00, 04:40, 08:00, 11:15, 12:55, 17:50, 19:30, 21:10, 22:50
June 4, 2001	05:15, 06:55, 08:35, 10:15, 13:30, 15:10, 16:50, 18:30, 21:45, 23:25

## Figure Captions.

Fig. 1. Comparison of the mean brightness temperatures of illuminated and shadowy pixels. The overbar indicates averaging over  $(50 \text{ km})^2$  areas, and so each point represents the mean values for a  $(50 \text{ km})^2$  area. All figures are based on the 9410 areas in the examined 30 MODIS scenes that have a cloud coverage larger than 10%. (Areas with cloud coverage below 10% were not considered because of the large statistical uncertainties that may arise for them.)

Figure 2. Comparison of the mean  $0.86 \mu\text{m}$  reflectances of illuminated and shadowy portions of  $(50 \text{ km})^2$  areas.

Figure 3. Comparison of mean optical thicknesses retrieved at the illuminated and shadowy portions of  $(50 \text{ km})^2$  areas.

Figure 4. Comparison of mean effective particle radii retrieved at the illuminated and shadowy portions of  $(50 \text{ km})^2$  areas. The dashed line indicates a linear fit to the data.

Figure 5. Illustration of the concept of 1D effective particle radius retrievals. The figure displays the relationship between nadir cloud reflectances at  $0.86 \mu\text{m}$  and  $2.12 \mu\text{m}$ , which was calculated using 1D theory for three different droplet sizes. The sample calculations are for  $60^\circ$  solar zenith angle, completely transparent cloud-free air, and nonreflecting surface.

Figure 6. Comparison of mean water paths retrieved at the illuminated and shadowy portions of  $(50 \text{ km})^2$  areas.

Figure 7. Dependence of 3D effects on the  $(50 \text{ km})^2$  average cloud optical thickness. The

relative difference ( $D_r$ ) is calculated as  $D_r = \frac{(\overline{WP}_i - \overline{WP}_s)}{\left(\frac{\overline{WP}_i + \overline{WP}_s}{2}\right)} \cdot 100\%$ . The solid line shows

the local mean values at  $\tau$ -steps of 2.5, and the error bars indicate the uncertainty of these mean values.

Figure 8. Dependence of the overall average water path of illuminated and shadowy pixels on cloud top pressure. The dotted line indicates the difference  $WP_i - WP_s$ .

Figure 9. Dependence of  $D_r$  values (defined at Fig. 7) on the cloud over of  $(50 \text{ km})^2$  areas.

Figure 10. Dependence of the illuminated-shadowy differences on the distance to the nearest cloud-free pixel. The relative difference is calculated as in Figs. 7 and 8, but combining all  $(1 \text{ km})^2$  pixels in all 30 examined scenes (instead of combining only pixels in individual  $(50 \text{ km})^2$  areas). The values displayed at a distance of 10 km represent the results for all distances greater than 8 km.

Figures.

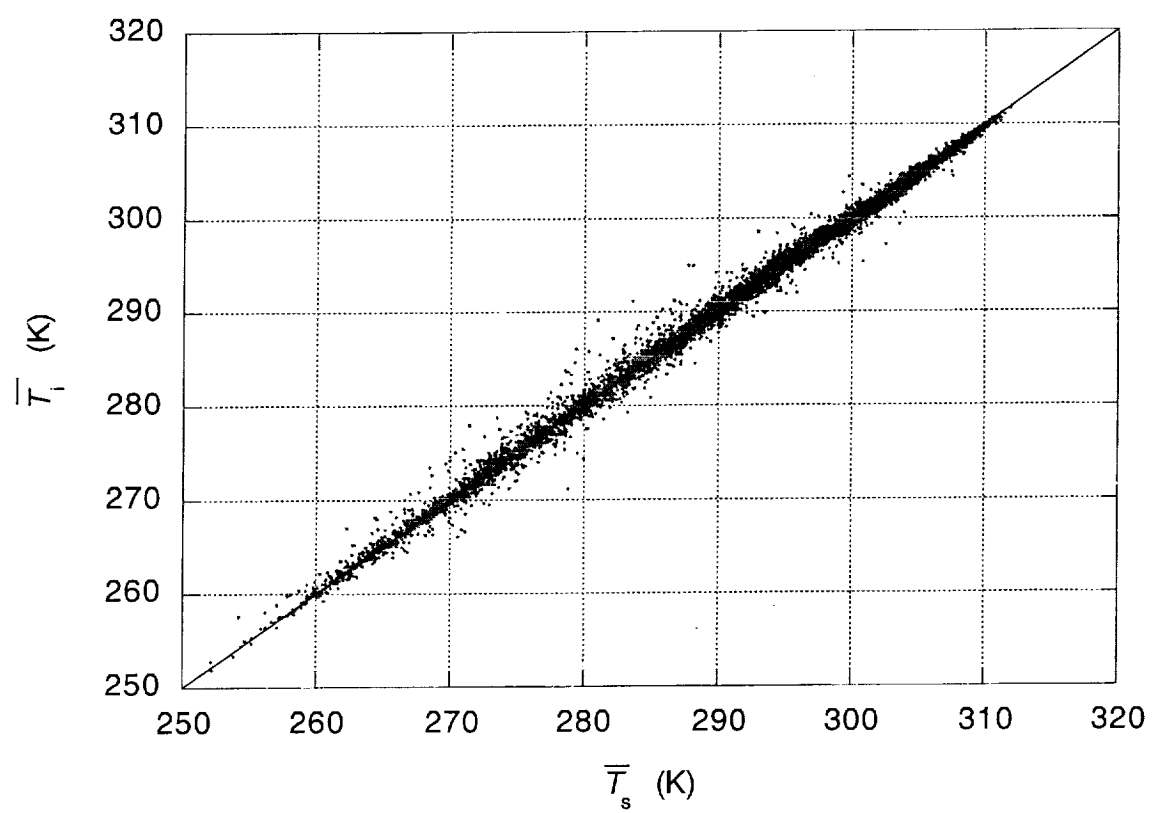


Figure 1.

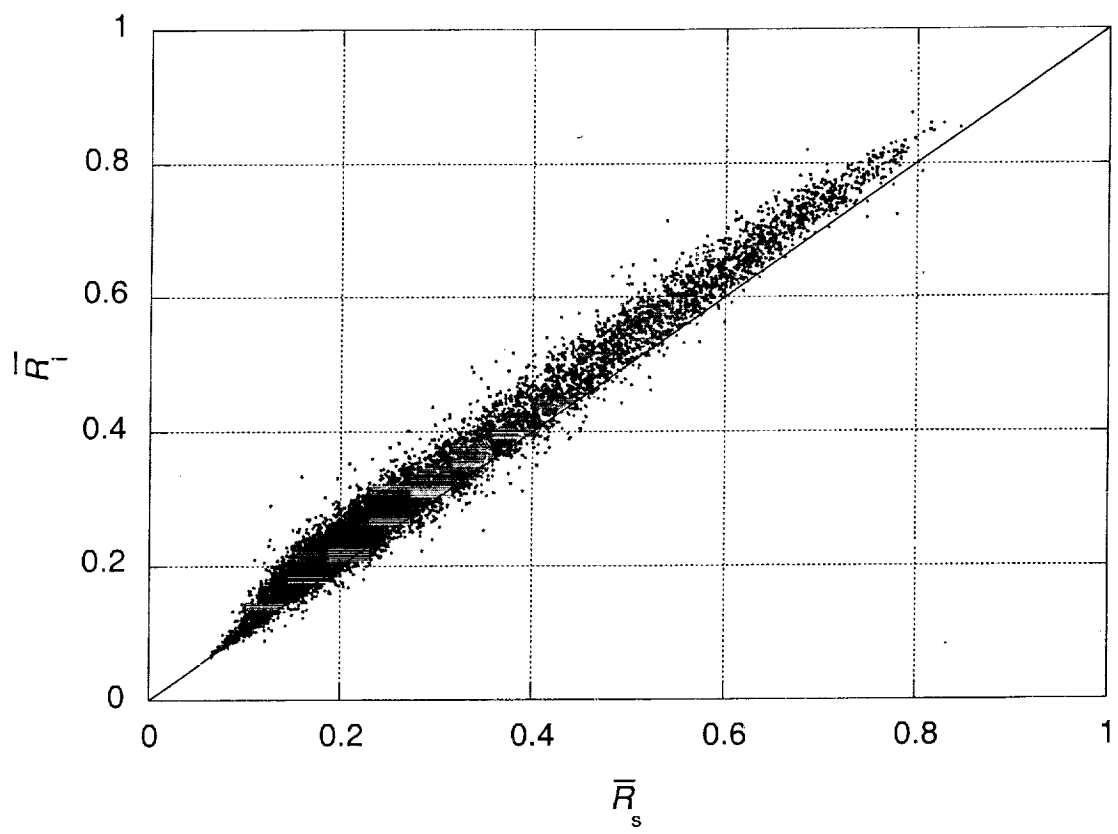


Figure 2.

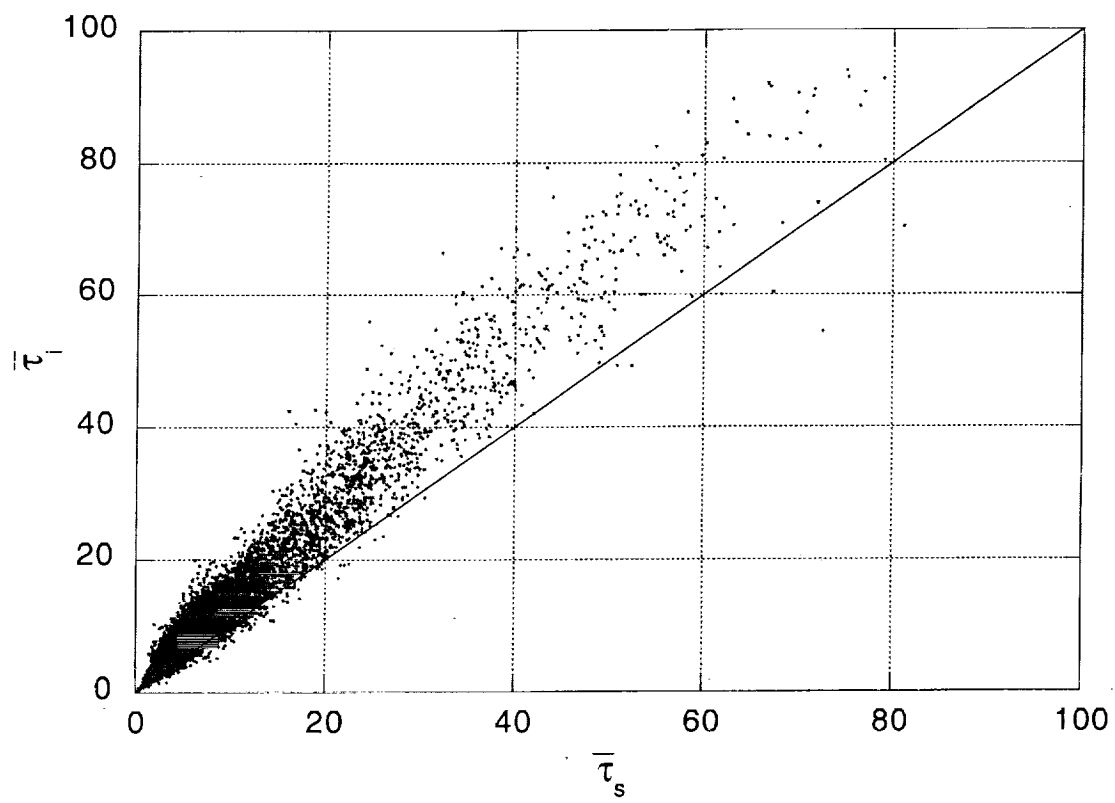


Figure 3.

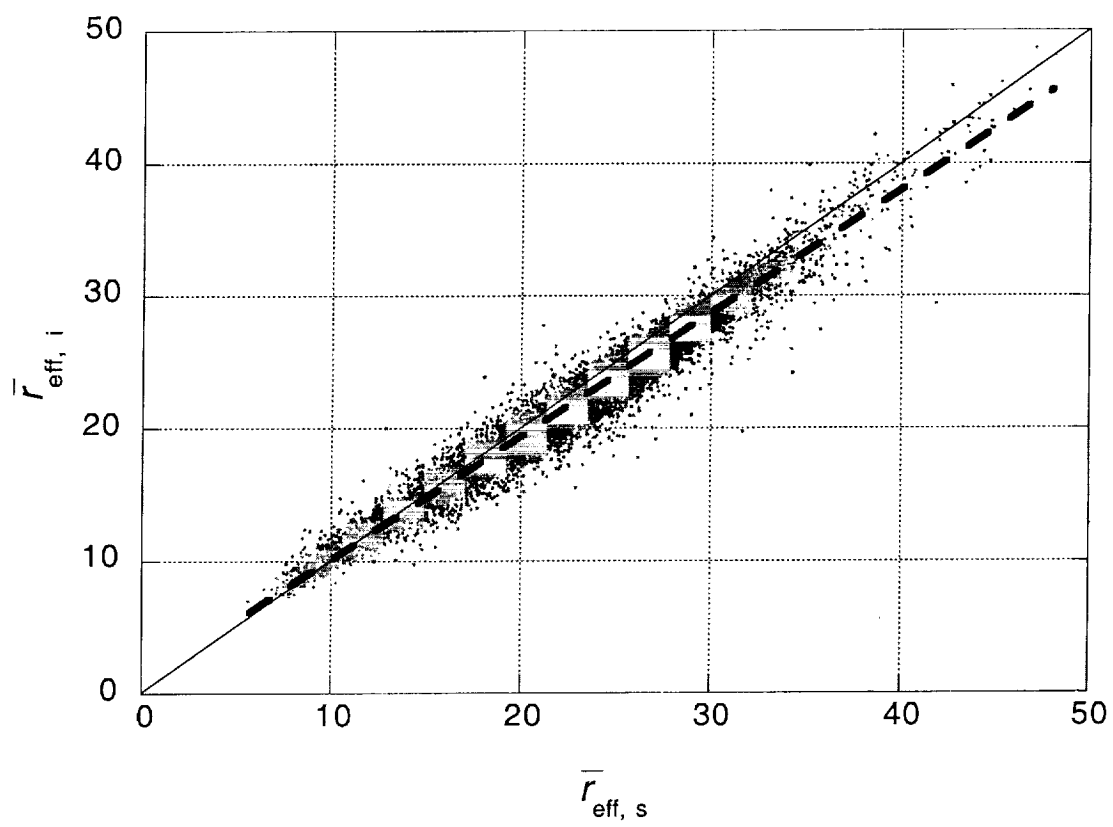


Figure 4.

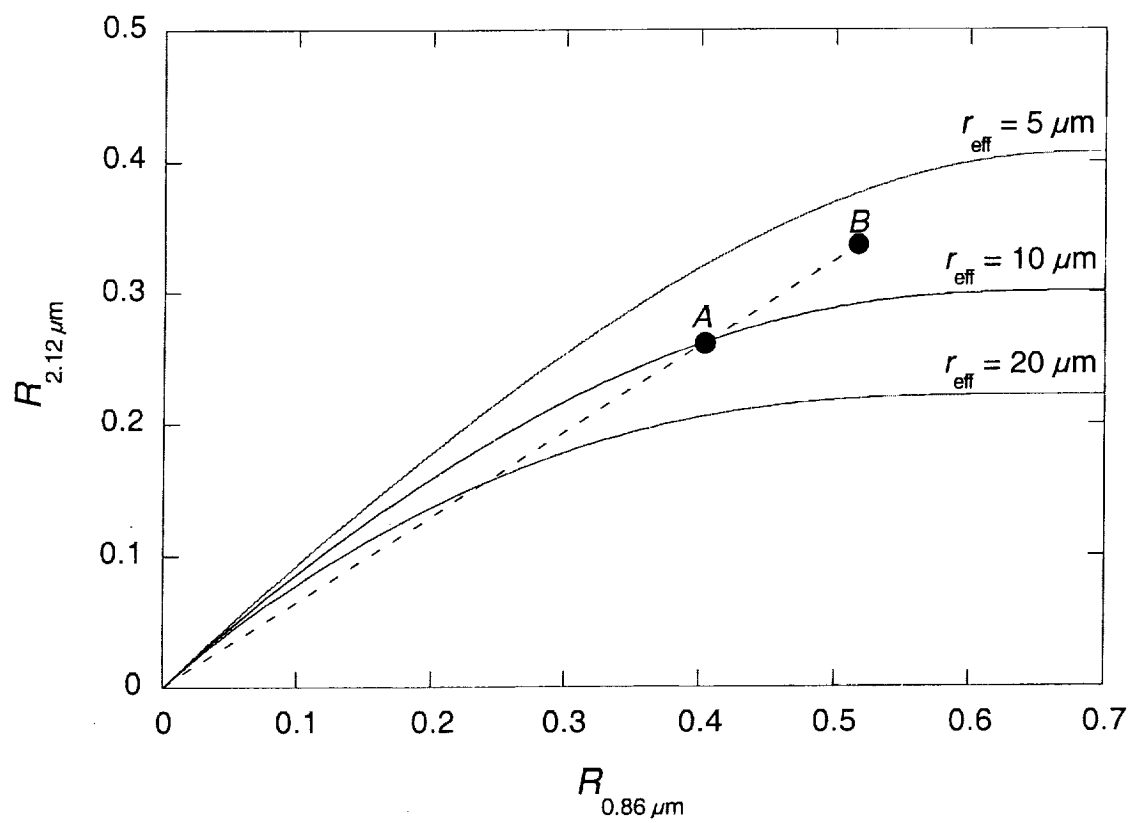


Figure 5.

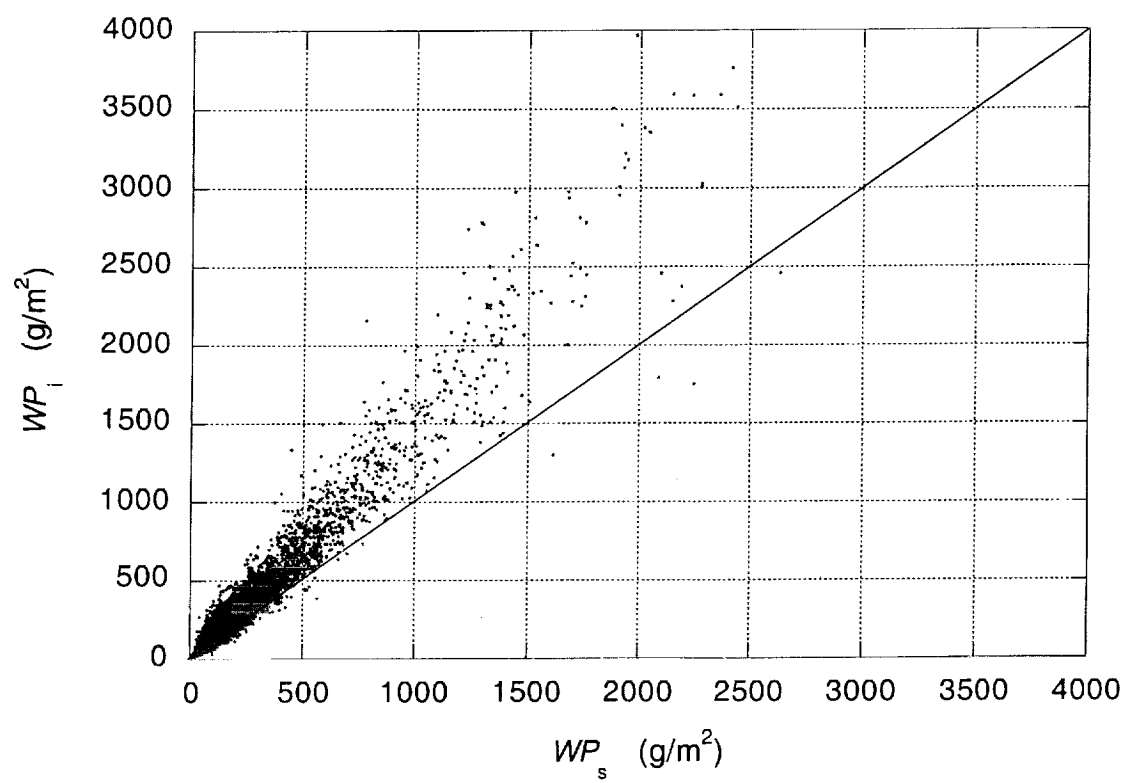


Figure 6.

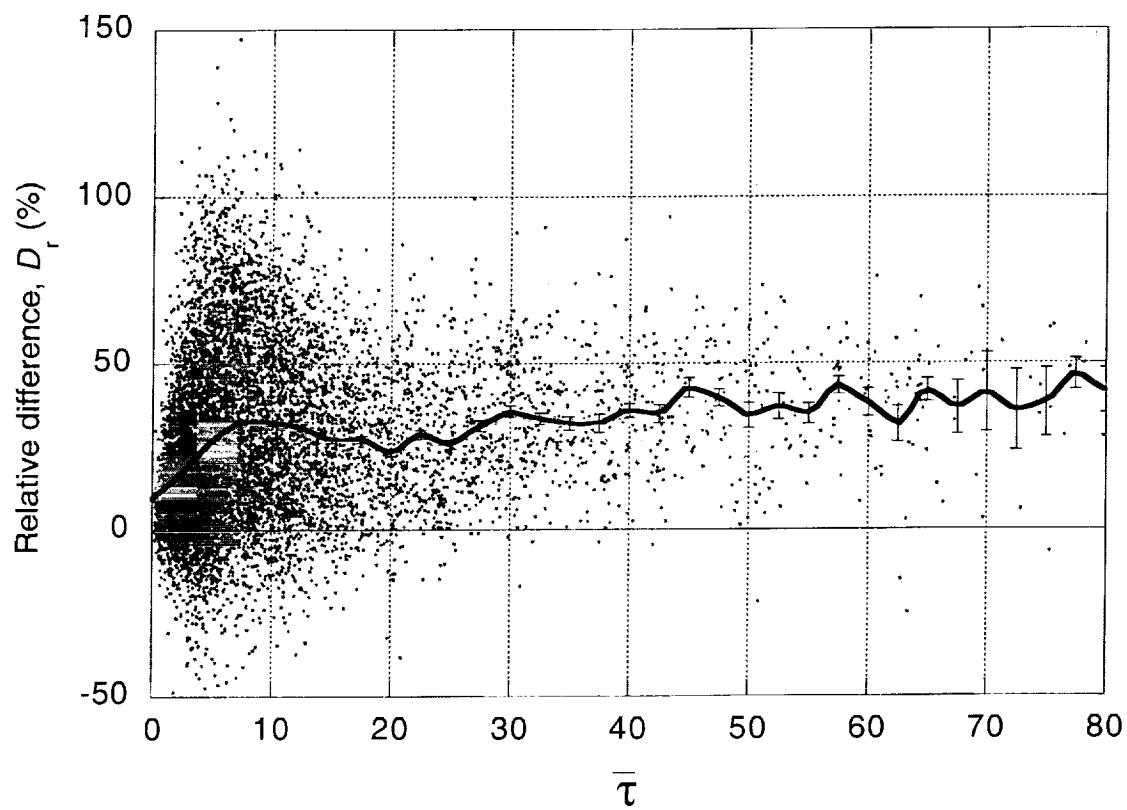


Figure 7.

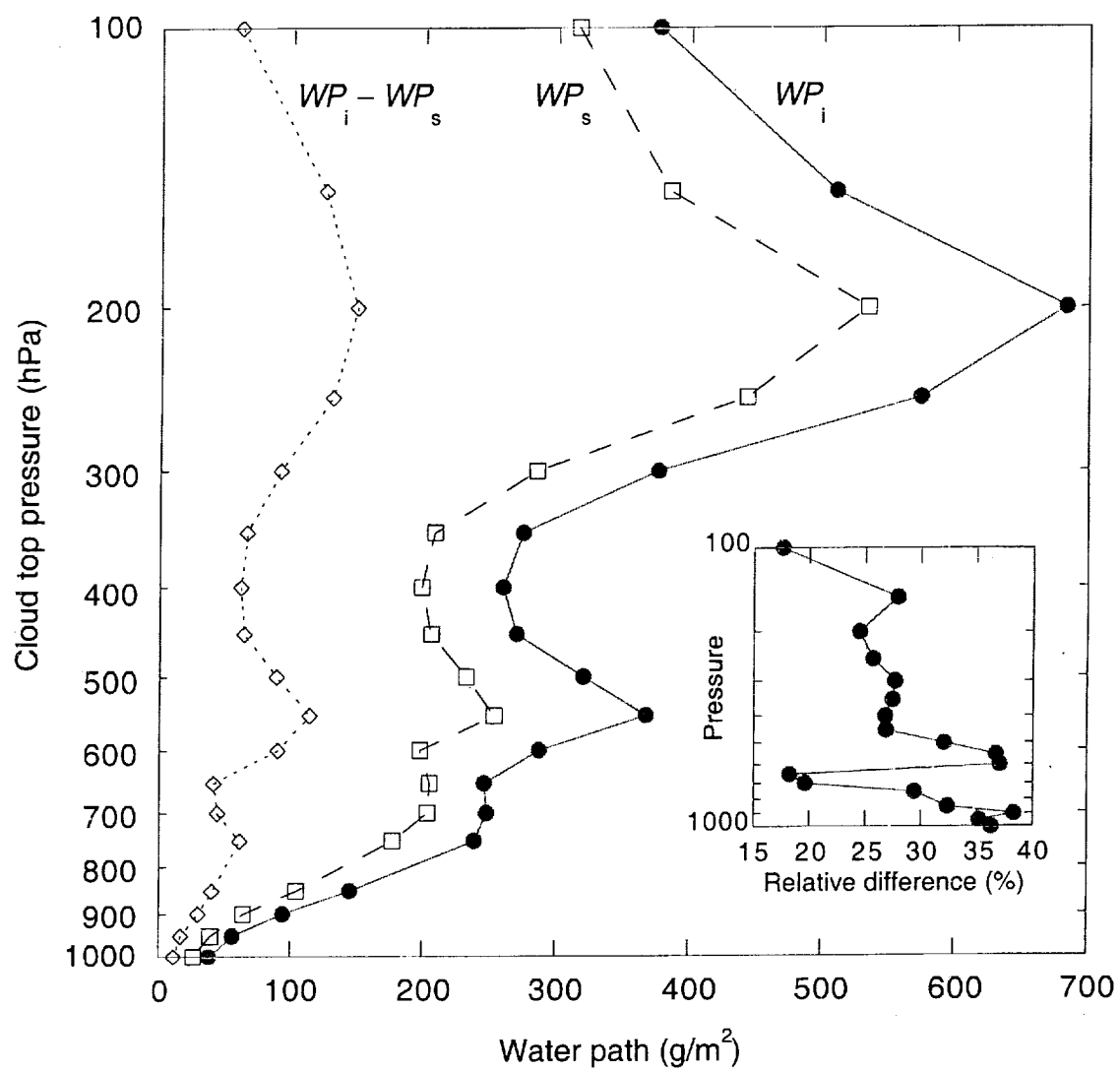


Figure 8.

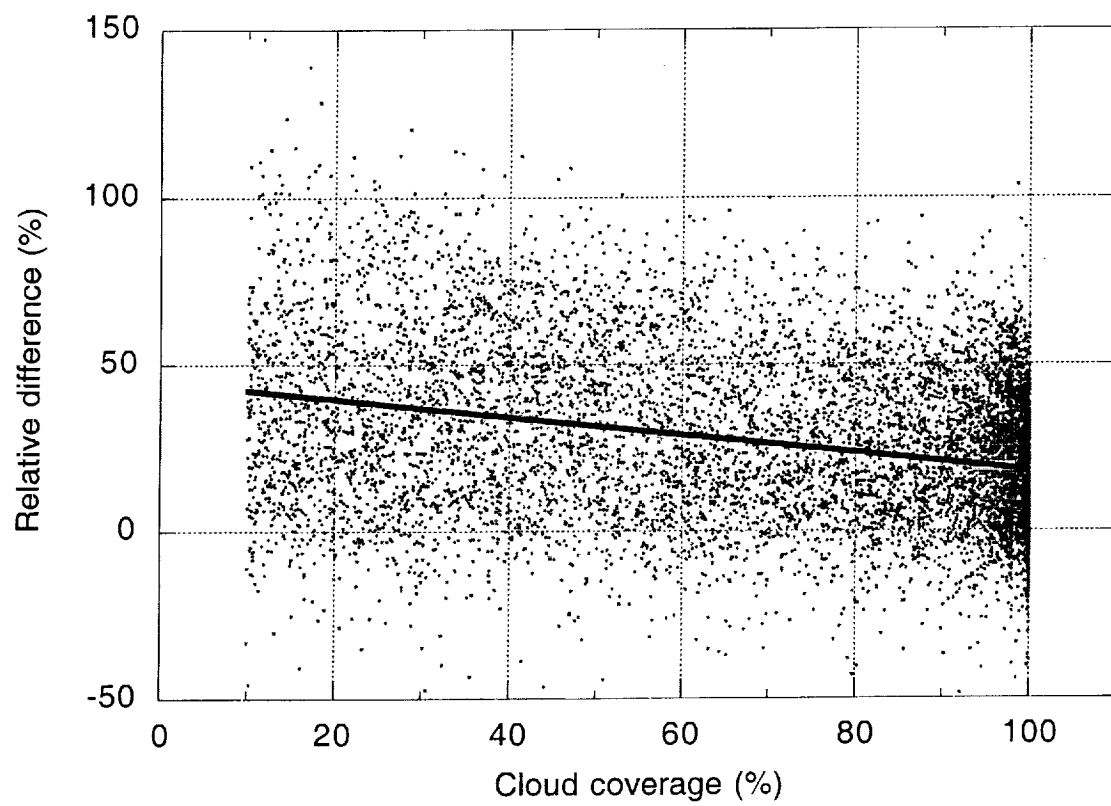


Figure 9.

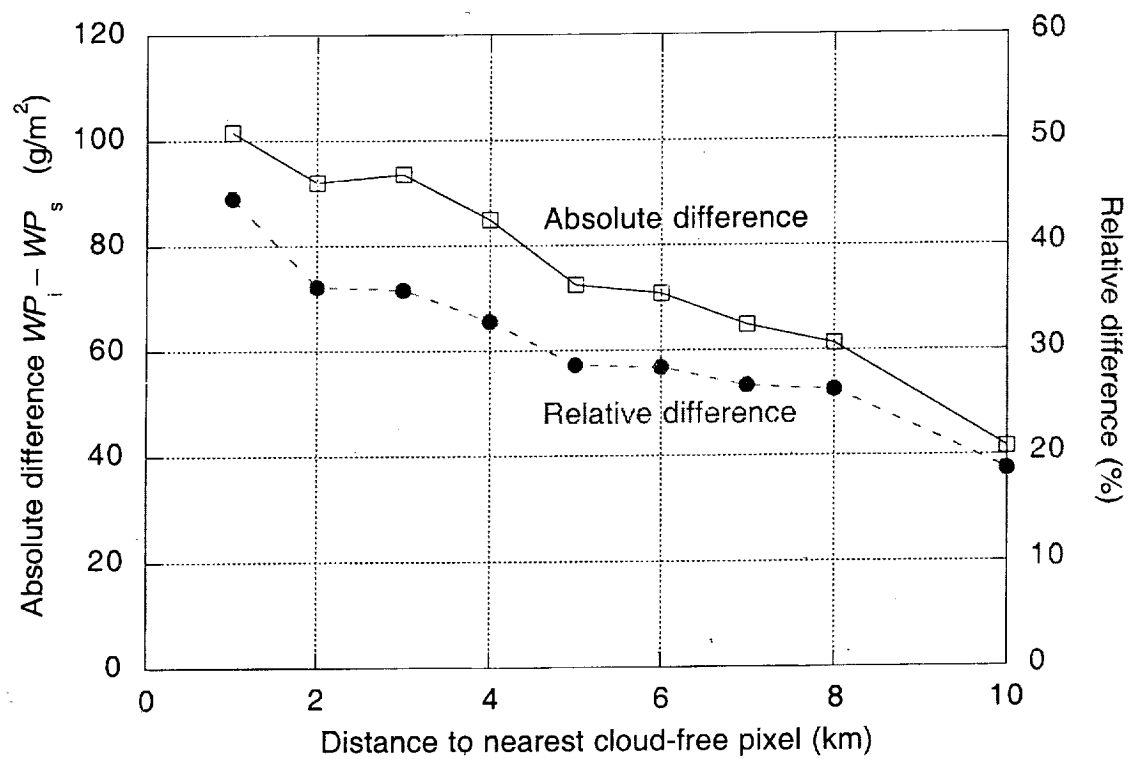


Figure 10.